

RESEARCH ARTICLE

Age-related estimates of aggregate g -ratio of white matter structures assessed using quantitative magnetic resonance neuroimaging

Mustapha Bouhrara¹  | Richard W. Kim¹ | Nikkita Khattar¹ | Wenshu Qian¹ | Christopher M. Bergeron¹ | Denise Melvin² | Linda M. Zukley² | Luigi Ferrucci³ | Susan M. Resnick⁴ | Richard G. Spencer¹

¹Laboratory of Clinical Investigation, National Institute on Aging, National Institutes of Health, Baltimore, Maryland

²Clinical Research Core, Office of the Scientific Director, National Institute on Aging, National Institutes of Health, Baltimore, Maryland

³Translational Gerontology Branch, National Institute on Aging, National Institutes of Health, Baltimore, Maryland

⁴Laboratory of Behavioral Neuroscience, National Institute on Aging, National Institutes of Health, Baltimore, Maryland

Correspondence

Mustapha Bouhrara, MRPAD Unit, National Institutes of Health (NIH), National Institute on Aging (NIA), Intramural Research Program, BRC 04B-117, 251 Bayview Boulevard, Baltimore, MD 21224, USA.
Email: bouhraram@mail.nih.gov

Funding information

National Institute on Aging

Abstract

The g -ratio, defined as the inner-to-outer diameter of a myelinated axon, is associated with the speed of nerve impulse conduction, and represents an index of axonal myelination and integrity. It has been shown to be a sensitive and specific biomarker of neurodevelopment and neurodegeneration. However, there have been very few magnetic resonance imaging studies of the g -ratio in the context of normative aging; characterizing regional and time-dependent cerebral changes in g -ratio in cognitively normal subjects will be a crucial step in differentiating normal from abnormal microstructural alterations. In the current study, we investigated age-related differences in aggregate g -ratio, that is, g -ratio averaged over all fibers within regions of interest, in several white matter regions in a cohort of 52 cognitively unimpaired participants ranging in age from 21 to 84 years. We found a quadratic, U-shaped, relationship between aggregate g -ratio and age in most cerebral regions investigated, suggesting myelin maturation until middle age followed by a decrease at older ages. As expected, we observed that these age-related differences vary across different brain regions, with the frontal lobes and parietal lobes exhibiting slightly earlier ages of minimum aggregate g -ratio as compared to more posterior structures such as the occipital lobes and temporal lobes; this agrees with the retrogenesis paradigm. Our results provide evidence for a nonlinear association between age and aggregate g -ratio in a sample of adults from a highly controlled population. Finally, sex differences in aggregate g -ratio were observed in several cerebral regions, with women exhibiting overall lower values as compared to men; this likely reflects the greater myelin content in women's brain, in agreement with recent investigations.

KEYWORDS

aggregate g -ratio, normal aging, quantitative MRI

Mustapha Bouhrara, Richard W. Kim, and Nikkita Khattar contributed equally to this study.

This is an open access article under the terms of the Creative Commons Attribution-NonCommercial-NoDerivs License, which permits use and distribution in any medium, provided the original work is properly cited, the use is non-commercial and no modifications or adaptations are made.

© 2021 The Authors. *Human Brain Mapping* published by Wiley Periodicals LLC.

1 | INTRODUCTION

Emerging evidence indicates that myelination and axonal abnormalities could lead to alterations in brain connectivity, contributing to a myriad of neurological disorders such as multiple sclerosis and Alzheimer's disease (Arfanakis, Gui, Tamhane, & Carew, 2007; Borich, MacKay, Vavasour, Rauscher, & Boyd, 2013; Bouhrara et al., 2018; Fjell et al., 2009; Flynn et al., 2003; Laule et al., 2008; MacKay & Laule, 2016). Studies have demonstrated that the *g*-ratio is highly correlated with the speed of neuronal signal conduction with conduction velocity increasing with myelin thickness (Chomiak & Hu, 2009; Rushton, 1951; Waxman, 1980). Thus, subtle changes in the *g*-ratio could modulate cognitive function and behavior. Furthermore, ex-vivo animal studies have indicated sex differences in the *g*-ratio secondary to hormonal differences, especially testosterone (Pesaresi et al., 2015). However, sex differences in *g*-ratio remain to be established in humans.

Electron microscopy is the gold standard technique to measure the *g*-ratio; this limits investigations to ex vivo measures. To address this, new clinical magnetic resonance imaging (MRI)-based methods have been introduced for whole-brain in vivo mapping of the *g*-ratio and have shown that the *g*-ratio could represent a sensitive and specific biomarker of neurodevelopment and neurodegeneration (Berman, West, Does, Yeatman, & Mezer, 2018; Campbell et al., 2017; Cercignani et al., 2017; Colgan et al., 2016; Dean et al., 2016; Mustafi et al., 2019; Parker et al., 2018; Yu et al., 2019). The original approach was introduced by Stikov and colleagues and is based on measuring the axonal and myelin volume fractions in a voxel, instead of for individual fibers, and assuming a uniform *g*-ratio for all fibers (Stikov et al., 2011); this has come to be known as the "aggregate *g*-ratio" (Stikov et al., 2015), the calculation of which requires an estimation of myelin volume fraction (MVF) and axonal volume fraction (AVF). Based on this notion, various MRI methods for measuring the aggregate *g*-ratio have more recently been introduced, incorporating a variety of approaches for estimating MVF or AVF (Campbell et al., 2017; Cercignani et al., 2017; Dean et al., 2016; Ellerbrock & Mohammadi, 2018; Jung et al., 2018; Mohammadi et al., 2015; West et al., 2018; Yu et al., 2019). Indeed, magnetization transfer (MT) imaging and multicomponent relaxometry have been used to estimate the MVF, while diffusion tensor imaging (DTI) and neurite orientation and dispersion density imaging (NODDI) have been used to estimate the AVF (Campbell et al., 2017; Cercignani et al., 2017; Dean et al., 2016; Ellerbrock & Mohammadi, 2018; Jung et al., 2018; MacKay & Laule, 2016; Mohammadi et al., 2015; Stikov et al., 2015; West et al., 2018; Yu et al., 2019). The advantages and limits of these techniques are discussed in detail in an excellent review by Campbell et al. (2017).

Age is the main risk factor for degenerative central nervous system disease and associated cognitive and functional impairment. It is, therefore, crucial to characterize microstructural changes, including in *g*-ratio, that occur with normal aging to distinguish them from changes caused by disease. In a recent study, Dean and colleagues investigated differences in aggregate *g*-ratio index across early neurodevelopment in children of ages between 3 months and 7.5 years (Dean et al., 2016), and reported logarithmically decreasing trends with age,

in agreement with the notion of rapid early brain maturation (Dean et al., 2015; Deoni, Dean, O'Muircheartaigh, Dirks, & Jerskey, 2012). In a pioneering MRI study, conducted on a cohort of adult subjects spanning a wide age range, based on MT and NODDI imaging, Cercignani and colleagues have found that the aggregate *g*-ratio increases linearly with age (Cercignani et al., 2017), interpreted as reduction in myelin throughout adulthood and decreased axonal density at older ages. However, this is difficult to reconcile with reports of increased myelination throughout adulthood followed by a decrease at older ages (Arshad, Stanley, & Raz, 2016; Bouhrara, Cortina, et al., 2020; Bouhrara, Rejimon, et al., 2020; Dvorak et al., 2021; Qian, Khattar, Cortina, Spencer, & Bouhrara, 2020). As discussed by the authors, this discrepancy is likely due to use of MT imaging for the estimation of MVF which, while sensitive to myelin content, is not specific, as well as to other technical considerations, including a limited cohort size.

In the current study, our main goal is to investigate age-related differences in aggregate *g*-ratio using emerging advanced techniques, namely, Bayesian Monte Carlo (BMC) mcDESPOt for MVF estimation (Bouhrara & Spencer, 2015, 2016, 2017) and NODDI, a multi-shell diffusion technique, for AVF estimation (Zhang, Schneider, Wheeler-Kingshott, & Alexander, 2012). Our study was conducted on a cohort of cognitively unimpaired participants spanning a wide age range.

2 | MATERIAL & METHODS

2.1 | Participants

Participants were drawn from two ongoing cohorts at the National Institute on Aging (NIA). Volunteers recruited from the Baltimore Longitudinal Study of Aging (BLSA) (Ferrucci, 2008; Shock, 1985), and from the Genetic and Epigenetic Signatures of Translational Aging Laboratory Testing (GESTALT) were enrolled. The study populations, experimental design, and measurement protocols of the BLSA have previously been reported (Ferrucci, 2008; Shock, 1985). The BLSA is a longitudinal cohort study funded and conducted by the NIA Intramural Research Program (IRP). Established in 1958, the BLSA enrolls community-dwelling adults with no major chronic conditions or functional impairments. The GESTALT study is also a study of healthy volunteers, initiated in 2015, funded, and conducted by the NIA IRP. The goal of the BLSA and GESTALT studies is to evaluate multiple biomarkers related to aging. We note that the inclusion and exclusion criteria for these two studies are essentially identical. Participants underwent testing at the NIA's clinical research unit and were excluded if they had metallic implants, neurologic, or medical disorders (O'Brien et al., 2009). Further, all participants underwent a Mini Mental State Examination (MMSE) and seven cognitively impaired participants were excluded. The final cohort consisted of 52 volunteers ranging in age from 21 to 84 years (44.6 ± 18.1 years), of which 24 were men (43.1 ± 17.5 years) and 28 were women (46.3 ± 18.6 years). Figure 1a provides a detailed distribution of the number of participants per age decade and for each sex. The mean \pm SD MMSE and education years (EDY) values of this cohort were 29.1

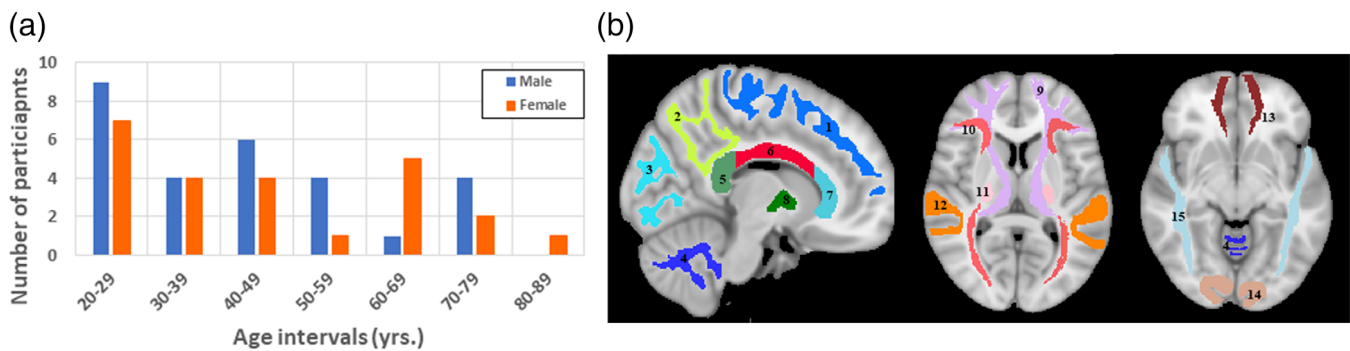


FIGURE 1 (a) Number of participants per age decade and sex. (b) Visualization of the white matter ROIs used in our analysis. 1) Frontal lobes, 2) Parietal lobes, 3) Occipital lobes, 4) Cerebellum, 5) Splenium of corpus callosum, 6) Body of corpus callosum, 7) Genu of corpus callosum, 8) Internal capsule, 9) Anterior thalamic radiation, 10) Corticospinal tract, 11) Inferior fronto-occipital fasciculus, 12) Temporal lobes, 13) Forceps minor, 14) Forceps major, 15) Inferior longitudinal fasciculus

± 1.2 and 15.3 ± 2.4 years, respectively. Age, MMSE, and EDY did not differ significantly between men and women. Experimental procedures were performed in compliance with our local Institutional Review Board, and participants provided written informed consent.

2.2 | Data acquisition

MRI scans were performed using a 3T Philips MRI system (Achieva, Best, The Netherlands). All participants underwent BMC-mcDESPOT for myelin water fraction (MWF) mapping and NODDI for intracellular volume fraction (ICVF) mapping imaging scans.

The BMC-mcDESPOT protocol consisted of 3D spoiled gradient recalled echo (SPGR) images acquired with flip angles (FAs) of $[2\ 4\ 6\ 8\ 10\ 12\ 14\ 16\ 18\ 20]^\circ$, echo time (TE) of 1.37 ms, repetition time (TR) of 5 ms, and acquisition time of ~ 5 min, as well as 3D balanced steady state free precession (bSSFP) images acquired with FAs of $[2\ 4\ 7\ 11\ 16\ 24\ 32\ 40\ 50\ 60]^\circ$, TE of 2.8 ms, TR of 5.8 ms, and acquisition time of ~ 6 min. The bSSFP images were acquired with radiofrequency (RF) excitation pulse phase increments of 0 or π in order to account for off-resonance effects (Deoni, 2011). All SPGR and bSSFP images were acquired with an acquisition matrix of $150 \times 130 \times 94$, and voxel size of $1.6\ \text{mm} \times 1.6\ \text{mm} \times 1.6\ \text{mm}$. Further, we used the double-angle method (DAM) to correct for excitation RF inhomogeneity (Stollberger & Wach, 1996). For that, two fast spin-echo images were acquired with FAs of 45° and 90° , TE of 102 ms, TR of 3,000 ms, acquisition voxel size of $2.6\ \text{mm} \times 2.6\ \text{mm} \times 4\ \text{mm}$, and acquisition time of ~ 4 min. The total acquisition time for this entire imaging protocol was ~ 21 min.

The NODDI protocol consisted of diffusion weighted images (DWI) acquired with single shot EPI with TR of 10,000 ms, TE of 67 ms, and three b -values of 0, 700, and 2000 s/mm^2 , with the latter two encoded in 32 directions, and acquisition voxel size of $2\ \text{mm} \times 2\ \text{mm} \times 3\ \text{mm}$. Two images at $b = 0\ \text{s}/\text{mm}^2$ were acquired. The acquisition time was ~ 12 min.

All images were obtained with field of view of $240\ \text{mm} \times 208\ \text{mm} \times 150\ \text{mm}$ and reconstructed to a voxel size of $2\ \text{mm} \times 2\ \text{mm} \times 2\ \text{mm}$.

We emphasize that all MRI studies and ancillary measurements were performed with the same MRI system, running the same pulse sequences, at the same facility, and directed by the same investigators for both BLSA and GESTALT participants.

2.3 | Image registration and parameter mapping

As noted, the g -ratio is defined as the inner-to-outer diameter of a myelinated axon; its calculation requires estimation of myelin volume fraction (MVF) and axonal volume fraction (AVF).

2.3.1 | MVF mapping

Using the FSL software (Jenkinson, Beckmann, Behrens, Woolrich, & Smith, 2012), all SPGR, bSSFP, and DAM images were linearly registered to the SPGR image obtained at FA of 8° and the derived transformation matrix was then applied to the SPGR, bSSFP, and DAM images for each participant. Then, a MWF map was generated using the BMC-mcDESPOT analysis from the registered SPGR, bSSFP, and DAM datasets (Bouhrara & Spencer, 2016, 2017). Briefly, BMC-mcDESPOT assumes a two-component non-exchanging system consisting of slowly relaxing and more rapidly relaxing components. The short component corresponds to the signal of water trapped within the myelin sheets while the long component corresponds to intra/extra cellular water. Analysis was performed explicitly accounting for nonzero TE as incorporated into the TE-corrected-mcDESPOT signal model (Bouhrara & Spencer, 2015). The MWF map derived using BMC-mcDESPOT was then converted to a corresponding MVF map using the geometrical analysis suggested by Jung and colleagues (Jung et al., 2018).

2.3.2 | AVF mapping

For each participant, the diffusion weighted (DW) images were corrected for eddy current and motion effects using the affine

registration tools implemented in FSL. Then, the DW images were registered to the averaged DW images obtained with $b = 0 \text{ s/mm}^2$, and the derived transformation matrix was then applied to the DW images. The ICVF map was derived from the registered DW images using NODDI (Zhang et al., 2012), a multi-shell diffusion technique which enables the estimation of three separate water compartments, namely, intracellular volume fraction (ICVF), extracellular volume fraction, and cerebrospinal fluid volume fraction (CSFVF). ICVF and CSFVF calculation from the NODDI dataset was conducted using the NODDI MATLAB toolbox available at <http://mig.cs.ucl.ac.uk/index.php?n=Tutorial.NODDI matlab>. Then, an AVF map was calculated from the MVF, the CSFVF, and the ICVF maps as follow: $AVF = (1 - MVF) \times (1 - CSFVF) \times ICVF$ (Campbell et al., 2017; Cercignani et al., 2017; Jung et al., 2018).

2.3.3 | Aggregate g -ratio mapping

For each participant, the averaged DW image obtained at $b = 0 \text{ s/mm}^2$ was registered to the co-registered averaged SPGR image over FAs using the affine registration technique implemented in FSL (Jenkinson et al., 2012). The calculated transformation matrix was then applied to the AVF map. The aggregate g -ratio map was then calculated from the spatially aligned MVF and AVF maps (Campbell et al., 2017; Cercignani et al., 2017; Dean et al., 2016; Jung et al., 2018) as follow:

$$\text{Aggregate } g\text{-ratio} = \sqrt{\frac{AVF}{AVF + MVF}}$$

2.4 | Image segmentation

After thorough visual inspection of data quality for each participant, the scalp, ventricles, and other nonparenchymal regions within the images were eliminated using the BET tool as implemented in the FSL software (Smith, 2002). Using the FNIRT tool as implemented in FSL (Jenkinson et al., 2012), the averaged SPGR image over FAs for each participant was nonlinearly registered to the Montreal Neurological Institute (MNI) standard space image and the derived transformation matrix was then applied to the aggregate g -ratio, AVF, and MVF maps for that corresponding participant. Sixteen white matter (WM) regions of interest (ROIs) were defined from MNI corresponding to regions previously identified as the focus of our investigation (Arshad et al., 2016; Faizy et al., 2018; Uddin, Figley, Solar, Shatil, & Figley, 2019) (Figure 1b). These ROIs correspond to whole brain (WB) WM, frontal lobes (FL) WM, parietal lobe (PL) WM, occipital lobe (OL) WM, temporal lobe (TL) WM, cerebellum (CRB) WM, splenium of corpus callosum (SCC), body of corpus callosum (BCC), genu of corpus callosum (GCC), internal capsule (IC), anterior thalamic radiation (ATR), inferior fronto-occipital fasciculus (IFOF), inferior longitudinal fasciculus (ILF), forceps major (FM), forceps minor (Fm), and corticospinal tract (CST). All ROIs were eroded to reduce partial

volume effects and imperfect image registration using the FSL tool *fslmaths*. Finally, for each ROI and each participant, the mean aggregate g -ratio, AVF, and MVF values were calculated.

2.5 | Statistical analysis

For each ROI, the effects of age and sex on aggregate g -ratio, AVF, or MVF were investigated using multiple linear regression with the mean aggregate g -ratio, AVF, or MVF within the ROI as the dependent variable and sex, age, and age² as independent variables, after mean age centering. The initial model incorporated interactions between sex and age as well as sex and age², but interaction terms were removed if found not to be significant. The resulting parsimonious model was then constructed without the nonsignificant interactions. In all cases, the threshold for statistical significance was $p < .05$ after correction for multiple ROI comparisons using the false discovery rate (FDR) method (Benjamini, 2010). All calculations were performed with MATLAB (MathWorks, Natick, MA).

3 | RESULTS

Figure 2 shows aggregate g -ratio, MVF, and AVF maps for representative participants of three different ages. Results are shown for two representative axial slices covering the main WM brain structures investigated. Visual inspection indicates decreases in aggregate g -ratio values from early adulthood until middle age (i.e., 40–49 years), followed by increases in aggregate g -ratio through older age in several brain regions. Moreover, visual inspection indicates increases in MVF until middle age followed by decreases afterward, while AVF shows a mostly decreasing pattern with age. Furthermore, we note that different regions exhibit different patterns of association between aggregate g -ratio, MWF, or AVF and age, as expected.

Figure 3 shows quantitative results for aggregate g -ratio values obtained from all participants as a function of age for the indicated 16 cerebral WM regions. As shown, there is a decrease in aggregate g -ratio until middle age followed by an increase with age in most ROIs examined, in agreement with visual inspection of Figure 2. The best-fit curves indicate that while the fundamental U-shaped relationship between aggregate g -ratio and age was consistent across these ROIs, there was notable regional variation. Indeed, the corpus callosum and the forceps minor ROIs exhibited minimal variations in aggregate g -ratio with age.

The effect of age on aggregate g -ratio was significant ($p < .05$) in five ROIs (Table 1). The quadratic effect of age on aggregate g -ratio was also significant in several brain structures (Table 1). Furthermore, our statistical analyses indicate that all ROIs exhibited nonsignificant interactions between age² and sex. Interaction between age and sex was nominally significant in a few brain regions, but these relationships did not survive the FDR correction; these regions were the whole brain WM, the temporal lobes WM, the cerebellum WM, and the body of the CC. In these regions, women showed a nonsignificant

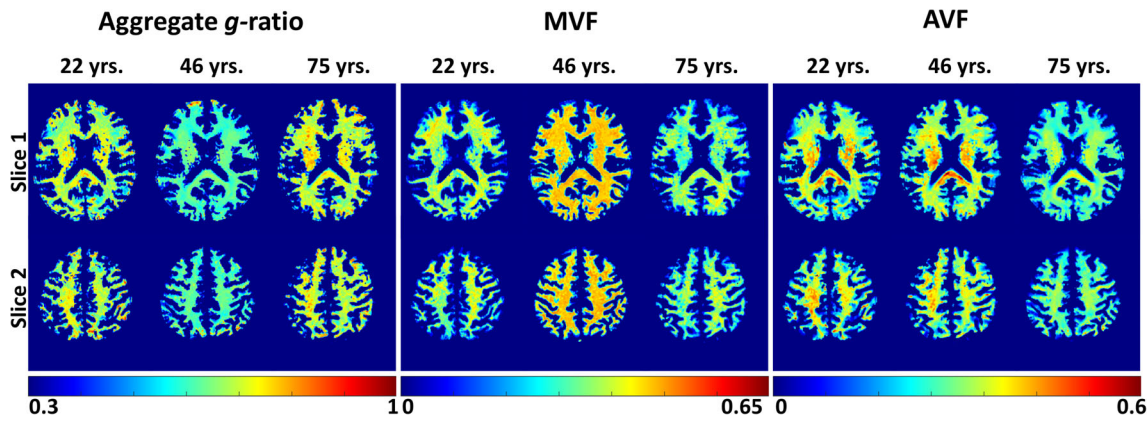


FIGURE 2 Aggregate *g*-ratio, MVF, and AVF maps derived from the brains of three women participants of different ages. For each participant, results are shown for two representative slices. AVF, axonal volume fraction; MVF, myelin volume fraction

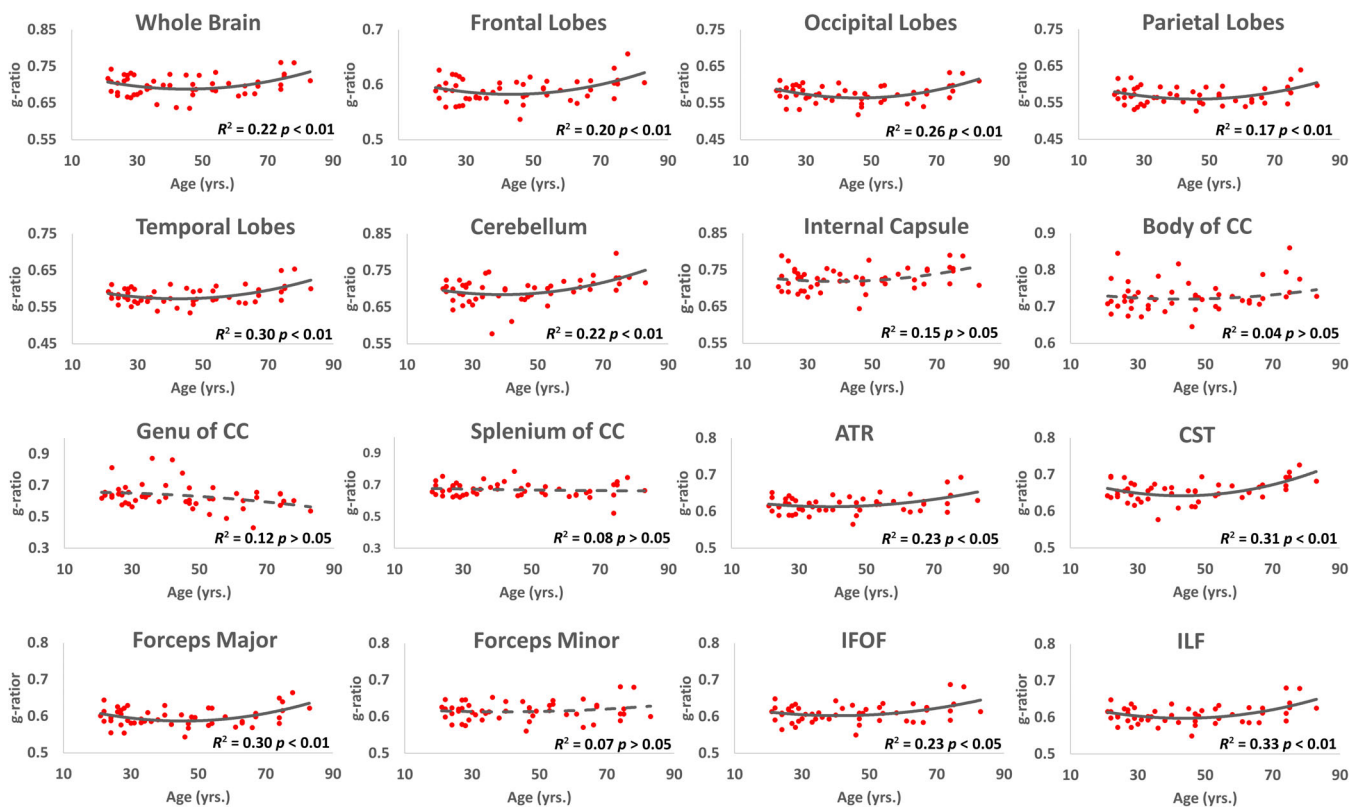


FIGURE 3 Plots of aggregate *g*-ratio values as a function of age ($N = 52$). Results are shown for the 16 white matter cerebral structures evaluated. For each region, the significance of the overall regression model, p , and corresponding coefficient of determination, R^2 , are reported. The solid black lines represent the best-fit curves when the overall regression is significant ($p < .05$) while the dashed black lines represent the best-fit curves when the overall regression is not significant ($p > .05$). Most regions investigated show a quadratic, U-shaped, association of aggregate *g*-ratio with age

trend to greater increase in aggregate *g*-ratio with age as compared to men. Furthermore, most of the brain structures evaluated exhibited minimum aggregate *g*-ratio values within the fifth age decade, that is, between 40 and 49 years. Interestingly, anterior and middle brain structures such as the frontal lobes WM and parietal lobes WM exhibited slightly earlier ages of minimum aggregate *g*-ratio as compared to more posterior structures such as the occipital lobes WM

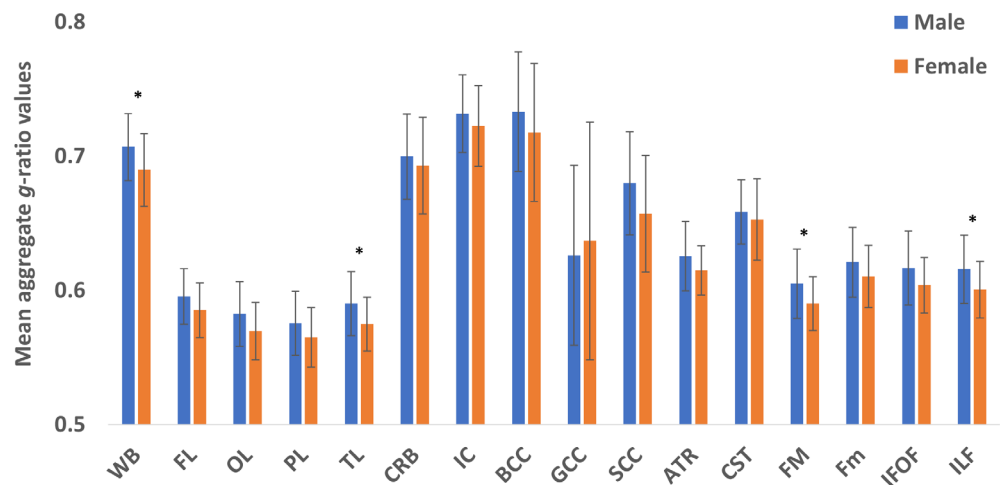
and temporal lobes WM (Table 1). Finally, a significant effect of sex on aggregate *g*-ratio was observed in four brain structures (Table 1), with women showing, overall, lower aggregate *g*-ratio values as compared to men (Figure 4).

Figure 5 shows quantitative results for AVF (Figure 5a) and MVF (Figure 5b) values obtained as a function of age for the indicated 16 cerebral WM regions. Visual inspection shows that most ROIs

TABLE 1 Significance of aggregate g -ratio results based on age, sex, and age²

	Age		Sex		Age ²		Year of minimum aggregate g -ratio
	p	F	p	F	p	F	
Whole brain	>.1	2.5	<.05	7.3	<.05	7.9	44.6
Frontal lobes	<.1	4.4	<.1	4.6	<.05	7.1	42.8
Occipital lobes	>.1	2.4	<.1	5.9	<.01	14.6	45.8
Parietal lobes	>.1	1.9	<.1	3.7	<.05	9.5	45.5
Temporal lobes	<.05	8.5	<.05	9.8	<.01	10.8	42.0
Cerebellum	<.05	8.7	>.1	1.2	<.05	5.3	38.9
Internal capsules	>.1	3.5	>.1	1.8	>.1	3.0	NA
Body of corpus callosum	>.1	0.3	>.1	1.4	>.1	0.5	NA
Genu of corpus callosum	<.1	5.8	>.1	0.5	>.1	0.3	NA
Splenium of corpus callosum	>.1	0.4	<.1	3.5	>.1	0.0	NA
Anterior thalamic radiation	<.05	6.8	<.1	4.8	>.1	3.3	NA
Corticospinal tract	<.05	7.4	>.1	1.8	<.01	10.7	39.3
Forceps major	>.1	1.5	<.05	8.1	<.05	6.5	52.0
Forceps minor	>.1	0.6	>.1	2.9	>.1	0.2	NA
Inferior fronto-occipital fasciculus	<.1	4.5	<.1	5.6	>.1	2.9	NA
Inferior longitudinal fasciculus	<.1	4.2	<.05	9.0	<.05	6.4	49.5

Note: Significance of regression terms in the multiple linear regression analysis, and year of apparent minimum aggregate g -ratio value for each brain structure investigated. NA indicates that the linear model was the best fit to the data, with the age of minimum aggregate g -ratio therefore occurring at the youngest or oldest age decade. Bold indicates significance ($p < .05$); all p -values presented are obtained after FDR correction.

FIGURE 4 Comparison of the mean aggregate g -ratio values for men and women in the ROIs studied. Mean aggregate g -ratio values for women are overall lower than mean aggregate g -ratio values for men. * indicates $p < .05$ 

exhibited decreasing AVF with age, in agreement with visual inspection of Figure 2. However, visual inspection of several structures, including the whole brain WM, frontal lobes WM, temporal lobes WM, cerebellum, ATR, ILF, and FM, indicated quadratic, inverted U-shaped, associations with age, while other ROIs, including the body of the CC, splenium, and CST, exhibit constant trends with age. The best-fit curves indicate that the AVF versus age curves displayed regional variation. Further, visual inspection shows increasing MVF until middle age followed by a decrease in MVF values with age in all ROIs examined, in agreement with visual inspection of Figure 2. The best-fit curves indicate that while the fundamental quadratic, inverted

U-shaped, relationship between MVF and age was consistent across all ROIs, there was some regional variation among these curves.

The effect of age on AVF was significant in seven ROIs (Table 2). The quadratic effect of age, that is, age², on AVF was not significant for any brain structure examined after FDR correction. Further, the effect of sex on AVF was not significant in any of the brain structures examined after FDR correction. Our statistical analyses indicate that all ROIs exhibited nonsignificant interactions between age² and sex, or age and sex. Finally, the effect of age on MVF was not significant in any of the ROIs after FDR correction (Table 2). The quadratic effect of age, that is, age², on MVF was significant in most brain structures

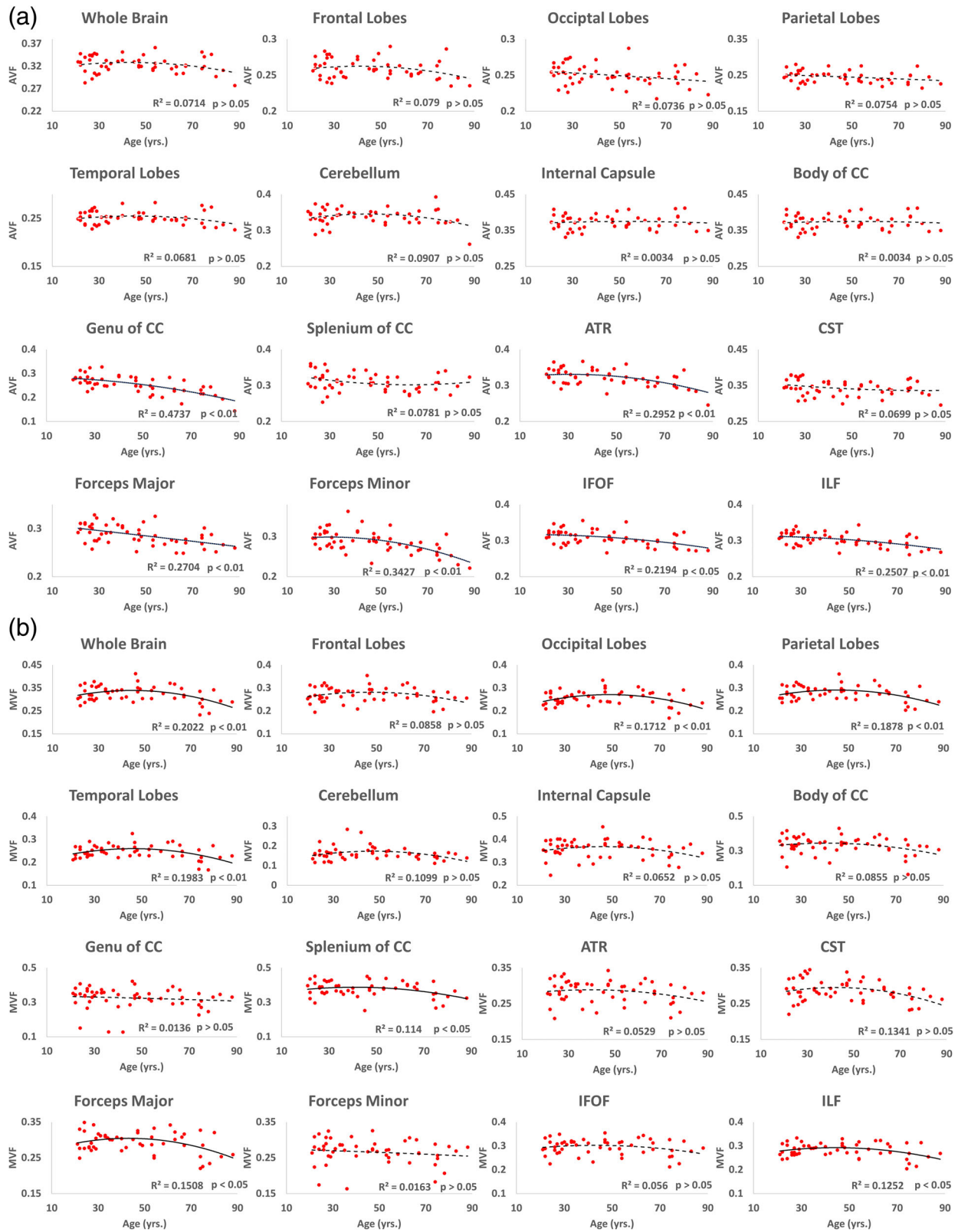


FIGURE 5 Plots of (a) AVF and (b) MVF values as a function of age ($N = 52$). Results are shown for the 16 white matter cerebral structures evaluated. For each region, the significance of the overall regression model, p , and corresponding coefficient of determination, R^2 , are reported. Solid black lines represent the best-fit curves when the overall regression is significant ($p < .05$) while the dashed black lines represent the best-fit curves when the overall regression is not significant ($p > .05$). AVF, axonal volume fraction; MVF, myelin volume fraction

TABLE 2 Significance of axonal volume fraction (AVF) and myelin volume fraction (MVF) results based on age, sex, and age²

	AVF						MVF					
	Age		Sex		Age ²		Age		Sex		Age ²	
	<i>p</i>	<i>F</i>	<i>p</i>	<i>F</i>	<i>p</i>	<i>F</i>	<i>p</i>	<i>F</i>	<i>p</i>	<i>F</i>	<i>p</i>	<i>F</i>
Whole brain	>.1	1.6	>.1	0.1	>.1	2.0	>.1	6.1	>.1	4.9	<.05	7.9
Frontal lobes	>.1	2.2	>.1	0.0	>.1	1.8	>.1	1.0	>.1	2.3	<.1	3.8
Occipital lobes	<.1	3.7	>.1	0.0	>.1	0.0	>.1	1.1	<.1	5.8	<.05	9.9
Parietal lobes	<.1	3.9	>.1	0.1	>.1	0.0	>.1	5.1	<.1	6.4	<.05	8.0
Temporal lobes	>.1	0.9	>.1	0.0	>.1	2.5	>.1	4.3	<.1	9.1	<.05	10.1
Cerebellum	>.1	1.1	>.1	1.2	>.1	3.9	>.1	1.2	>.1	2.6	<.05	5.1
Internal capsules	>.1	0.0	>.1	0.3	>.1	0.1	>.1	1.1	>.1	1.5	<.1	3.7
Body of corpus callosum	<.05	6.3	>.1	2.1	>.1	0.0	>.1	3.1	>.1	1.3	>.1	1.8
Genu of corpus callosum	<.01	42.5	>.1	0.8	>.1	1.2	>.1	0.8	>.1	0.5	>.1	0.0
Splenium of corpus callosum	>.1	2.6	>.1	0.8	>.1	1.2	>.1	4.7	>.1	4.1	<.1	3.5
Anterior thalamic radiation	<.01	17.9	>.1	0.0	>.1	3.4	>.1	2.1	>.1	1.1	>.1	1.0
Corticospinal tract	>.1	3.4	>.1	0.0	>.1	0.2	>.1	4.2	>.1	0.9	<.1	3.9
Forceps major	<.01	19.7	>.1	0.8	>.1	0.0	>.1	5.0	>.1	3.2	<.05	5.0
Forceps minor	<.01	23.2	>.1	0.0	>.1	3.4	>.1	1.0	>.1	0.6	>.1	0.0
Inferior fronto-occipital fasciculus	<.01	13.6	>.1	0.0	>.1	0.7	>.1	1.7	>.1	1.8	>.1	1.6
Inferior longitudinal fasciculus	<.01	16.6	>.1	0.1	>.1	0.6	>.1	3.4	>.1	4.3	<.05	4.8

Note: Significance of regression terms in the multiple linear regression analysis for each brain structure investigated. Bold indicates significance ($p < 0.05$); all p -values presented are obtained after FDR correction.

evaluated. Further, the effect of sex on MVF was not significant in any of the brain structures studied after FDR correction. Our statistical analyses indicate that all ROIs exhibited nonsignificant interactions between age² and sex, or age and sex.

4 | DISCUSSION

4.1 | Aggregate g -ratio

In this work, we investigated differences in aggregate g -ratio across adult lifespan. Our analysis was conducted on a cohort of cognitively unimpaired participants spanning a wide age-range. Our aggregate g -ratio mapping method showed a high degree of sensitivity to aggregate g -ratio differences with age, with derived values spanning a relatively large dynamic range, from 0.55 and 0.8, reflecting substantial structural variation across the brain. This is in good agreement with literature (Berman et al., 2018; Cercignani et al., 2017; Chomiak & Hu, 2009). Indeed, theoretical and experimental work suggests that the optimal g -ratio is within that range (Berman et al., 2018; Cercignani et al., 2017; Chomiak & Hu, 2009).

Our results indicate a quadratic, U-shape, association between aggregate g -ratio and age in most white matter regions analyzed (Table 1 and Figure 3). These results are consistent with a pattern of brain maturation through middle age followed by a rapid decline, in agreement with postmortem observations (Peters, 2002; Tang, Nyengaard, Pakkenberg, & Gundersen, 1997). Indeed, previous studies have revealed inverted U-shape trends of MWF with age in different brain structures (Arshad

et al., 2016; Bouhrara, Cortina, et al., 2020; Bouhrara, Rejimon, et al., 2020; Dvorak et al., 2021); although MWF represents a very different metric than aggregate g -ratio, both of these indices are expected to correlate with overall extent and quality of myelination. In addition, we found that different regions exhibited similarities, as well as differences, in the associations between aggregate g -ratio and age, with most regions peaking during the fifth decade of life. This finding is in good agreement with several MRI studies based on diffusion tensor imaging and relaxometry (Bartzokis et al., 2010; Okubo et al., 2017; Westlye et al., 2010; Yeatman, Wandell, & Mezer, 2014). However, the corpus callosum subdivisions exhibited either no trend or a trend towards linearly decreasing aggregate g -ratio with age; this agrees with Berman and colleagues' observations (Berman et al., 2018). Furthermore, our results indicate a delay in minimum aggregate g -ratio development in the occipital lobes WM as compared to other regions. This pattern is in line with the retrogenesis hypothesis (first in-last out), in which posterior brain regions are spared from degeneration as compared to anterior brain regions (Bender, Völkle, & Raz, 2016; Brickman et al., 2012; Raz, 2000; Stricker et al., 2009). However, additional longitudinal studies are required to further validate this finding.

In a recent MRI study conducted to investigate age-related differences in aggregate g -ratio in the adult human brain (Cercignani et al., 2017), Cercignani and colleagues have observed that aggregate g -ratio appears to increase linearly with age in various cerebral white matter tracts (Cercignani et al., 2017), interpreted as reduction in myelin throughout adulthood and decreased axonal density at older ages. Our report of a quadratic relationship may be the result of a

different analytic approach, in which we explicitly explored nonlinear aggregate g -ratio trends with age, as well as methodological differences, and cohort size differences. Furthermore, our results, indicating that the corpus callosum exhibited minimal but statistically significant differences in aggregate g -ratio values with age as compared to the other regions investigated, largely agree with Berman and colleagues' observations indicating minimal differences in aggregate g -ratio with age in different substructures of the corpus callosum (Berman et al., 2018). Finally, it must be emphasized that all current MRI methods for mapping aggregate g -ratio operate under the assumption that g -ratio is constant for all axons within a given voxel; this assumption may not always hold, as the aggregate g -ratio measure has been shown to be more sensitive to larger diameter axons (West, Kelm, Carson, & Does, 2016). The advantages and limits of these techniques are discussed in detail by Campbell and colleagues (Campbell et al., 2017).

The emergence of a quadratic age trend, as well as the ages at which the local aggregate g -ratio achieves its minimum, will depend to a certain extent on sampling density within age groups, range of ages incorporated, and consistency of data (Fjell et al., 2010). Indeed, analysis of our data excluding participants over 70 years (data not shown) indicates that the quadratic associations between age and aggregate g -ratio persist in a limited number of brain regions including the whole brain, occipital lobes, parietal lobes, temporal lobes, cerebellum, CST, and ILF. The remaining regions exhibited mostly decreasing trends of aggregate g -ratio as a function of age. In addition, while the choice of a quadratic regression model is consistent with our visual inspection, it must be regarded as an expedient way to model the data, rather than a description of underlying physiologic processes. Other models, such as piecewise linear, may serve equally well as data descriptors. However, the present analysis provides a basic demonstration of aggregate g -ratio trends decreasing from early adulthood through middle age, with an increase thereafter.

We found statistically significant sex differences in aggregate g -ratio in several brain regions with women showing, overall, lower cerebral aggregate g -ratio values as compared to men (Table 1, Figure 4); this likely corresponds to the higher myelin content seen in women's brain (Arshad et al., 2016; Bouhrara, Cortina, et al., 2020; Bouhrara, Rejimon, et al., 2020). Our results agree with Pesaresi and colleagues' work indicating overall higher aggregate g -ratio values in male rats (Pesaresi et al., 2015). These trends indicate potential lines of investigation in larger cohorts. Indeed, sexual dimorphism in aggregate g -ratio are consistent with previous demonstrations that proliferation of oligodendrocytes and myelin proteins are regulated differently in men and women (49, 50). A recent study suggests that sex steroids may influence this differential regulation, possibly also contributing to sex differences in repair (51). However, it must be emphasized that the distribution of sex in our study cohort, particularly at the older ages, was not homogenous. Therefore, our sex-related results must be interpreted with caution.

4.2 | AVF and MVF

Although our results indicate decreasing trends of AVF with age in most white matter regions analyzed (Figure 5), various brain

structures exhibited apparent quadratic, inverted U-shaped, associations with age; this agrees with Cercignani and colleagues' observations (Cercignani et al., 2017). However, these quadratic associations were not statistically significant, although there were trends to significance before FDR correction. We conjecture that the lack of very young participants (<20 years old) in our cohort precluded adequate detection of this relationship; this limitation derives from the exclusion criteria of the BLSA and GESTALT studies. Inclusion of younger participants may influence the shape of AVF age-related trends. Further, our results indicate a quadratic association between MVF and age in all white matter regions (Table 2 and Figure 5b). These results agree with our and others' recent studies indicating an inverted U-shape association of myelin content with age in several white matter regions (Arshad et al., 2016; Bouhrara, Cortina, et al., 2020; Bouhrara, Rejimon, et al., 2020; Dvorak et al., 2021). The quadratic association between MVF and age is attributed to the process of myelination from youth through middle age, followed by demyelination in later years (Arshad et al., 2016; Bartzokis et al., 2010); this pattern is in agreement with postmortem observations (Peters, 2002; Tang et al., 1997). As expected, we found that different regions exhibit both similarities and differences in associations between MVF and age. This finding is in good agreement with several studies based on myelin-sensitive MRI methods such as diffusion tensor imaging and relaxation times (Bartzokis et al., 2010; Okubo et al., 2017; Westlye et al., 2010; Yeatman et al., 2014).

4.3 | Limitations

Although our cohort spanned a wide age range, it does not include participants younger than 20 years; this limitation derives from the exclusion criteria of the BLSA and GESTALT studies. Inclusion of younger participants may influence the shape of the age-related aggregate g -ratio trends as discussed above. We also note that it was not feasible to obtain fully uniform sampling across all age intervals in this convenience sample of participants in ongoing research protocols, with the number of participants aged 50–70 years being somewhat lower as compared to the other age decades. Further, our dataset is cross-sectional, so that the quadratic trends observed here require further validation through longitudinal studies. Such work, motivated by the present results, is underway. In addition, our results were obtained on cohorts of cognitively normal adults and results obtained in the setting of pathology may differ. Indeed, it has been shown that the presence of nonmyelinated axons could bias derived aggregate g -ratio values (West et al., 2018).

Moreover, due to the limited spatial resolution of the diffusion imaging datasets, contamination from cerebrospinal fluid as well as partial volume issues may have been introduced. Indeed, the voxel volume of the NODDI images is ~3 times higher than that of the BMC-mcDESPOT images, leading to ICVF maps with much lower spatial resolution as compared to the MWF maps (Figure 6). To mitigate the potential effects of partial volume contamination, all ROIs were eroded followed by careful visual inspection. Nevertheless, some

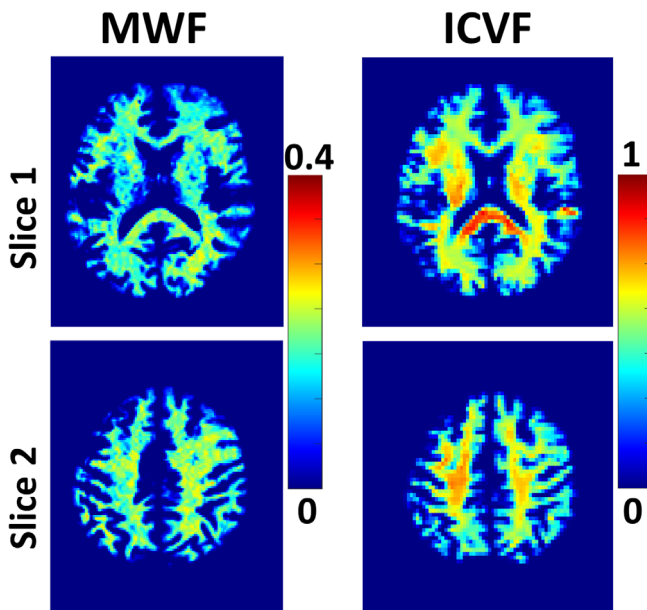


FIGURE 6 Example of MWF and ICVF maps generated at the acquisition voxel size of $1.6 \text{ mm} \times 1.6 \text{ mm} \times 1.6 \text{ mm}$ and $2 \text{ mm} \times 2 \text{ mm} \times 3 \text{ mm}$, respectively. These maps were generated from the images acquired from the brain of a 75-year-old participant. ICVF, intra-cellular volume fraction; MWF, myelin water fraction

partial volume effects could have persisted especially in small structures including the tracts. In addition, age-related tissue atrophy could lead to non-optimal image registration, potentially introducing some bias in derived aggregate g -ratio values. Nevertheless, visual inspection indicates that age-related tissue atrophy was limited to a very few participants belonging to the oldest age decade of our cohort. Further, the linear scaling suggested by Jung and colleagues, derived from the multi-gradient echo-based technique of MWF mapping, was used to compute MVF from MWF derived using BMC-mcDESPOT (Jung et al., 2018). However, further work is required to refine or validate this approach for MWF derived using BMC-mcDESPOT.

Finally, we note that mcDESPOT, including BMC-mcDESPOT, provides somewhat higher MWF values as compared to multiple spin echo (MSE)-based methods (Zhang, Kolind, Laule, & MacKay, 2015a). Various experimental and physiological factors which are not considered in the MSE or mcDESPOT signal models could account for this discrepancy. These include, but are not limited to, magnetization transfer between macromolecules and free water protons, longitudinal relaxation time effects resulting from use of short repetition times in MSE, iron content, exchange between water pools, J -coupling, off-resonance effects, spin locking, water diffusion within different compartments, and internal gradients. These represent major challenges in MR imaging studies of myelin content, with additional technical developments required to further improve accuracy. In addition, the NODDI model does not explicitly account for differing transverse relaxation times for different tissue compartments; the resulting echo-time-dependence has been shown to bias NODDI-derived outcomes (Gong et al., 2020). Indeed, all of the available quantitative models for

MVF and AVF determination incorporate simplifications dictated by technical and experimental considerations which likely to lead to biases in derived aggregate g -values (Alonso-Ortiz, Levesque, & Pike, 2015; Bouhrara et al., 2016; Bouhrara & Spencer, 2015; Campbell et al., 2017; Zhang et al., 2015a; Zhang, Kolind, Laule, & MacKay, 2015b). However, our analysis (data not shown) indicates that an overestimation of 10% in MVF or AVF leads to an underestimation or an overestimation of ~2% in aggregate g -ratio, respectively.

5 | CONCLUSIONS

We showed that aggregate g -ratio values follow a U-shaped trend with normal aging in several white matter structures of the human brain. We interpret this as indicating increased myelin content through middle age, followed by decrease in myelin content. These results agree with previous MRI studies that have investigated myelination in the aging brains of cognitively unimpaired participants.

ACKNOWLEDGMENT

This work was supported by the Intramural Research Program of the National Institute on Aging of the National Institutes of Health.

CONFLICT OF INTEREST

None.

DATA AVAILABILITY STATEMENT

All codes and data are available upon request from the corresponding author.

ORCID

Mustapha Bouhrara  <https://orcid.org/0000-0001-6184-669X>

REFERENCES

- Alonso-Ortiz, E., Levesque, I. R., & Pike, G. B. (2015). MRI-based myelin water imaging: A technical review. *Magnetic Resonance in Medicine*, 73(1), 70–81. <https://doi.org/10.1002/mrm.25198>
- Arfanakis, K., Gui, M., Tamhane, A. A., & Carew, J. D. (2007). Investigating the medial temporal lobe in Alzheimer's disease and mild cognitive impairment, with turboprop diffusion tensor imaging, MRI-volumetry, and T 2-relaxometry. *Brain Imaging and Behavior*, 1(1), 11–21. <https://doi.org/10.1007/s11682-007-9001-4>
- Arshad, M., Stanley, J. A., & Raz, N. (2016). Adult age differences in sub-cortical myelin content are consistent with protracted myelination and unrelated to diffusion tensor imaging indices. *NeuroImage*, 143, 26–39. <https://doi.org/10.1016/j.neuroimage.2016.08.047>
- Bartzokis, G., Lu, P. H., Tingus, K., Mendez, M. F., Richard, A., Peters, D. G., ... Mintz, J. (2010). Lifespan trajectory of myelin integrity and maximum motor speed. *Neurobiology of Aging*, 31(9), 1554–1562. <https://doi.org/10.1016/j.neurobiolaging.2008.08.015>
- Bender, A. R., Völkle, M. C., & Raz, N. (2016). Differential aging of cerebral white matter in middle-aged and older adults: A seven-year follow-up. *NeuroImage*, 125, 74–83. <https://doi.org/10.1016/j.neuroimage.2015.10.030>
- Benjamini, Y. (2010). Discovering the false discovery rate. *Journal of the Royal Statistical Society. Series B (Statistical Methodology)*, 72(4), 405–416. Retrieved from <http://www.jstor.org/stable/40802219>

- Berman, S., West, K. L., Does, M. D., Yeatman, J. D., & Mezer, A. A. (2018). Evaluating g-ratio weighted changes in the corpus callosum as a function of age and sex. *NeuroImage*, *182*, 304–313. <https://doi.org/10.1016/j.neuroimage.2017.06.076>
- Borich, M. R., MacKay, A. L., Vavasour, I. M., Rauscher, A., & Boyd, L. A. (2013). Evaluation of white matter myelin water fraction in chronic stroke. *NeuroImage: Clinical*, *2*, 569–580. <https://doi.org/10.1016/j.nicl.2013.04.006>
- Bouhrara, M., Cortina, L. E., Rejimon, A. C., Khattar, N., Bergeron, C., Bergeron, J., ... Spencer, R. G. (2020). Quantitative age-dependent differences in human brainstem myelination assessed using high-resolution magnetic resonance mapping. *NeuroImage*, *206*, 116307. <https://doi.org/10.1016/j.neuroimage.2019.116307>
- Bouhrara, M., Reiter, D., Bergeron, C., Zukley, L., Ferrucci, L., Resnick, S., & Spencer, R. (2018). Evidence of demyelination in mild cognitive impairment and dementia using a direct and specific magnetic resonance imaging measure of myelin content. *Alzheimer's & Dementia*, *14*(8), 998–1004. <https://doi.org/10.1016/j.jalz.2018.03.007>
- Bouhrara, M., Reiter, D. A., Celik, H., Fishbein, K. W., Kijowski, R., & Spencer, R. G. (2016). Analysis of mcDESPOT- and CPMG-derived parameter estimates for two-component nonexchanging systems. *Magnetic Resonance in Medicine*, *75*(6), 2406–2420. <https://doi.org/10.1002/mrm.25801>
- Bouhrara, M., Rejimon, A. C., Cortina, L. E., Khattar, N., Bergeron, C. M., Ferrucci, L., ... Spencer, R. G. (2020). Adult brain aging investigated using BMC-mcDESPOT based myelin water fraction imaging. *Neurobiology of Aging*, *85*, 131–139. <https://doi.org/10.1016/j.neurobiolaging.2019.10.003>
- Bouhrara, M., & Spencer, R. G. (2015). Incorporation of nonzero echo times in the SPGR and bSSFP signal models used in mcDESPOT. *Magnetic Resonance in Medicine*, *74*(5), 1227–1235. <https://doi.org/10.1002/mrm.25984>
- Bouhrara, M., & Spencer, R. G. (2016). Improved determination of the myelin water fraction in human brain using magnetic resonance imaging through Bayesian analysis of mcDESPOT. *NeuroImage*, *127*, 456–471. <https://doi.org/10.1016/j.neuroimage.2015.10.034>
- Bouhrara, M., & Spencer, R. G. (2017). Rapid simultaneous high-resolution mapping of myelin water fraction and relaxation times in human brain using BMC-mcDESPOT. *NeuroImage*, *147*, 800–811. <https://doi.org/10.1016/j.neuroimage.2016.09.064>
- Brickman, A. M., Meier, I. B., Korgaonkar, M. S., Provenzano, F. A., Grieve, S. M., Siedlecki, K. L., ... Zimmerman, M. E. (2012). Testing the white matter retrogenesis hypothesis of cognitive aging. *Neurobiology of Aging*, *33*(8), 1699–1715. <https://doi.org/10.1016/j.neurobiolaging.2011.06.001>
- Campbell, J. S. W., Leppert, I. R., Narayanan, S., Boudreau, M., Duval, T., Cohen-Adad, J., ... Stikov, N. (2017). Promise and pitfalls of g-ratio estimation with MRI. *NeuroImage*, *182*, 80–96. <https://doi.org/10.1016/j.neuroimage.2017.08.038>
- Cercignani, M., Giulietti, G., Dowell, N. G., Gabel, M., Broad, R., Leigh, P. N., ... Bozzali, M. (2017). Characterizing axonal myelination within the healthy population: A tract-by-tract mapping of effects of age and gender on the fiber g-ratio. *Neurobiology of Aging*, *49*, 109–118. <https://doi.org/10.1016/j.neurobiolaging.2016.09.016>
- Chomiak, T., & Hu, B. (2009). What is the optimal value of the g-ratio for myelinated fibers in the rat CNS? A theoretical approach. *PLoS One*, *4* (11), e7754. <https://doi.org/10.1371/journal.pone.0007754>
- Colgan, N., Siow, B., O'Callaghan, J. M., Harrison, I. F., Wells, J. A., Holmes, H. E., ... Lythgoe, M. F. (2016). Application of neurite orientation dispersion and density imaging (NODDI) to a tau pathology model of Alzheimer's disease. *NeuroImage*, *125*, 739–744. <https://doi.org/10.1016/j.neuroimage.2015.10.043>
- Dean, D. C., O'Muircheartaigh, J., Dirks, H., Travers, B. G., Adluru, N., Alexander, A. L., & Deoni, S. C. L. (2016). Mapping an index of the myelin g-ratio in infants using magnetic resonance imaging. *NeuroImage*, *132*, 225–237. <https://doi.org/10.1016/j.neuroimage.2016.02.040>
- Dean, D. C., O'Muircheartaigh, J., Dirks, H., Waskiewicz, N., Lehman, K., Walker, L., ... Deoni, S. C. (2015). Estimating the age of healthy infants from quantitative myelin water fraction maps. *Human Brain Mapping*, *36*(4), 1233–1244. <https://doi.org/10.1002/hbm.22671>
- Deoni, S. C. (2011). Correction of main and transmit magnetic field (B0 and B1) inhomogeneity effects in multicomponent-driven equilibrium single-pulse observation of T1 and T2. *Magnetic Resonance in Medicine*, *65*(4), 1021–1035. <https://doi.org/10.1002/mrm.22685>
- Deoni, S. C. L., Dean, D. C., O'Muircheartaigh, J., Dirks, H., & Jerskey, B. A. (2012). Investigating white matter development in infancy and early childhood using myelin water fraction and relaxation time mapping. *NeuroImage*, *63*(3), 1038–1053. <https://doi.org/10.1016/j.neuroimage.2012.07.037>
- Dvorak, A. V., Swift-LaPointe, T., Vavasour, I. M., Lee, L. E., Abel, S., Russell-Schulz, B., ... Kolind, S. H. (2021). An atlas for human brain myelin content throughout the adult life span. *Scientific Reports*, *11*(1), 269. <https://doi.org/10.1038/s41598-020-79540-3>
- Ellerbrock, I., & Mohammadi, S. (2018). Four in vivo g-ratio-weighted imaging methods: Comparability and repeatability at the group level. *Human Brain Mapping*, *39*(1), 24–41. <https://doi.org/10.1002/hbm.23858>
- Faizy, T. D., Kumar, D., Broocks, G., Thaler, C., Flottmann, F., Leischner, H., ... Gellißen, S. (2018). Age-related measurements of the myelin water fraction derived from 3D multi-echo GRASE reflect myelin content of the cerebral white matter. *Scientific Reports*, *8*(1), 14991. <https://doi.org/10.1038/s41598-018-33112-8>
- Ferrucci, L. (2008). The Baltimore longitudinal study of aging (BLSA): A 50-year-long journey and plans for the future. *The Journals of Gerontology. Series A, Biological Sciences and Medical Sciences*, *63*(12), 1416–1419.
- Fjell, A. M., Engvig, A., Tamnes, C. K., Grydeland, H., Walhovd, K. B., Westlye, L. T., ... Due-Tønnessen, P. (2009). Life-span changes of the human brain white matter: Diffusion tensor imaging (DTI) and volumetry. *Cerebral Cortex*, *20*(9), 2055–2068. <https://doi.org/10.1093/cercor/bhp280>
- Fjell, A. M., Walhovd, K. B., Westlye, L. T., Ostby, Y., Tamnes, C. K., Jernigan, T. L., ... Dale, A. M. (2010). When does brain aging accelerate? Dangers of quadratic fits in cross-sectional studies. *NeuroImage*, *50*(4), 1376–1383. <https://doi.org/10.1016/j.neuroimage.2010.01.061>
- Flynn, S. W., Lang, D. J., Mackay, A. L., Goghari, V., Vavasour, I. M., Whittall, K. P., ... Honer, W. G. (2003). Abnormalities of myelination in schizophrenia detected in vivo with MRI, and post-mortem with analysis of oligodendrocyte proteins. *Molecular Psychiatry*, *8*(9), 811–820. <https://doi.org/10.1038/sj.mp.4001337>
- Gong, T., Tong, Q., He, H., Sun, Y., Zhong, J., & Zhang, H. (2020). MTE-NODDI: Multi-TE NODDI for disentangling non-T2-weighted signal fractions from compartment-specific T2 relaxation times. *NeuroImage*, *217*, 116906. <https://doi.org/10.1016/j.neuroimage.2020.116906>
- Jenkinson, M., Beckmann, C. F., Behrens, T. E., Woolrich, M. W., & Smith, S. M. (2012). FSL. *NeuroImage*, *62*(2), 782–790. <https://doi.org/10.1016/j.neuroimage.2011.09.015>
- Jung, W., Lee, J., Shin, H. G., Nam, Y., Zhang, H., Oh, S. H., & Lee, J. (2018). Whole brain g-ratio mapping using myelin water imaging (MWI) and neurite orientation dispersion and density imaging (NODDI). *NeuroImage*, *182*, 379–388. <https://doi.org/10.1016/j.neuroimage.2017.09.053>
- Laule, C., Kozlowski, P., Leung, E., Li, D. K., Mackay, A. L., & Moore, G. R. (2008). Myelin water imaging of multiple sclerosis at 7 T: Correlations with histopathology. *NeuroImage*, *40*(4), 1575–1580. <https://doi.org/10.1016/j.neuroimage.2007.12.008>
- MacKay, A. L., & Laule, C. (2016). Magnetic resonance of myelin water: An in vivo marker for myelin. *Brain Plasticity*, *2*(1), 71–91.

- Mohammadi, S., Carey, D., Dick, F., Diedrichsen, J., Sereno, M. I., Reisert, M., ... Weiskopf, N. (2015). Whole-brain in-vivo measurements of the axonal G-ratio in a group of 37 healthy volunteers. *Frontiers in Neuroscience*, 9, 441–441. <https://doi.org/10.3389/fnins.2015.00441>
- Mustafi, S. M., Harezlak, J., Kodiweera, C., Randolph, J. S., Ford, J. C., Wishart, H. A., & Wu, Y.-C. (2019). Detecting white matter alterations in multiple sclerosis using advanced diffusion magnetic resonance imaging. *Neural Regeneration Research*, 14(1), 114–123. <https://doi.org/10.4103/1673-5374.243716>
- O'Brien, R. J., Resnick, S. M., Zonderman, A. B., Ferrucci, L., Crain, B. J., Pletnikova, O., ... Troncoso, J. C. (2009). Neuropathologic studies of the Baltimore longitudinal study of aging (BLSA). *Journal of Alzheimer's Disease*, 18(3), 665–675. <https://doi.org/10.3233/JAD-2009-1179>
- Okubo, G., Okada, T., Yamamoto, A., Fushimi, Y., Okada, T., Murata, K., & Togashi, K. (2017). Relationship between aging and T1 relaxation time in deep gray matter: A voxel-based analysis. *Journal of Magnetic Resonance Imaging*, 46(3), 724–731. <https://doi.org/10.1002/jmri.25590>
- Parker, T. D., Slatery, C. F., Zhang, J., Nicholas, J. M., Paterson, R. W., Foulkes, A. J. M., ... Schott, J. M. (2018). Cortical microstructure in young onset Alzheimer's disease using neurite orientation dispersion and density imaging. *Human Brain Mapping*, 39(7), 3005–3017. <https://doi.org/10.1002/hbm.24056>
- Pesaresi, M., Soon-Shiong, R., French, L., Kaplan, D. R., Miller, F. D., & Paus, T. (2015). Axon diameter and axonal transport: In vivo and in vitro effects of androgens. *NeuroImage*, 115, 191–201. <https://doi.org/10.1016/j.neuroimage.2015.04.048>
- Peters, A. (2002). The effects of normal aging on myelin and nerve fibers: A review. *Journal of Neurocytology*, 31(8–9), 581–593.
- Qian, W., Khattar, N., Cortina, L. E., Spencer, R. G., & Bouhrara, M. (2020). Nonlinear associations of neurite density and myelin content with age revealed using multicomponent diffusion and relaxometry magnetic resonance imaging. *NeuroImage*, 223, 117369. <https://doi.org/10.1016/j.neuroimage.2020.117369>
- Raz, N. (2000). Aging of the brain and its impact on cognitive performance: Integration of structural and functional findings. In *The handbook of aging and cognition* (2nd ed., pp. 1–90). Mahwah, NJ: Lawrence Erlbaum Associates.
- Rushton, W. A. H. (1951). A theory of the effects of fibre size in medullated nerve. *The Journal of Physiology*, 115(1), 101–122. <https://doi.org/10.1113/jphysiol.1951.sp004655>
- Shock, N. (1985). Normal human aging: The Baltimore longitudinal study of aging. *Journal of Gerontology*, 40(6), 767–774. <https://doi.org/10.1093/geronj/40.6.767>
- Smith, S. M. (2002). Fast robust automated brain extraction. *Human Brain Mapping*, 17(3), 143–155. <https://doi.org/10.1002/hbm.10062>
- Stikov, N., Campbell, J. S. W., Stroh, T., Lavelée, M., Frey, S., Novek, J., ... Pike, G. B. (2015). In vivo histology of the myelin g-ratio with magnetic resonance imaging. *NeuroImage*, 118, 397–405. <https://doi.org/10.1016/j.neuroimage.2015.05.023>
- Stikov, N., Perry, L. M., Mezer, A., Rykhlevskaia, E., Wandell, B. A., Pauly, J. M., & Dougherty, R. F. (2011). Bound pool fractions complement diffusion measures to describe white matter micro and macrostructure. *NeuroImage*, 54(2), 1112–1121. <https://doi.org/10.1016/j.neuroimage.2010.08.068>
- Stollberger, R., & Wach, P. (1996). Imaging of the active B1 field in vivo. *Magnetic Resonance in Medicine*, 35(2), 246–251.
- Stricker, N. H., Schweinsburg, B. C., Delano-Wood, L., Wierenga, C. E., Bangen, K. J., Haaland, K. Y., ... Bondi, M. W. (2009). Decreased white matter integrity in late-myelinating fiber pathways in Alzheimer's disease supports retrogenesis. *NeuroImage*, 45(1), 10–16. <https://doi.org/10.1016/j.neuroimage.2008.11.027>
- Tang, Y., Nyengaard, J. R., Pakkenberg, B., & Gundersen, H. J. (1997). Age-induced white matter changes in the human brain: A stereological investigation. *Neurobiology of Aging*, 18(6), 609–615.
- Uddin, M. N., Figley, T. D., Solar, K. G., Shatil, A. S., & Figley, C. R. (2019). Comparisons between multi-component myelin water fraction, T1w/T2w ratio, and diffusion tensor imaging measures in healthy human brain structures. *Scientific Reports*, 9(1), 2500. <https://doi.org/10.1038/s41598-019-39199-x>
- Waxman, S. G. (1980). Determinants of conduction velocity in myelinated nerve fibers. *Muscle & Nerve*, 3(2), 141–150. <https://doi.org/10.1002/mus.880030207>
- West, K. L., Kelm, N. D., Carson, R. P., Alexander, D. C., Gochberg, D. F., & Does, M. D. (2018). Experimental studies of g-ratio MRI in ex vivo mouse brain. *NeuroImage*, 167, 366–371. <https://doi.org/10.1016/j.neuroimage.2017.11.064>
- West, K. L., Kelm, N. D., Carson, R. P., & Does, M. D. (2016). A revised model for estimating g-ratio from MRI. *NeuroImage*, 125, 1155–1158. <https://doi.org/10.1016/j.neuroimage.2015.08.017>
- Westlye, L. T., Walhovd, K. B., Dale, A. M., Bjornerud, A., Due-Tønnessen, P., Engvig, A., ... Fjell, A. M. (2010). Life-span changes of the human brain white matter: Diffusion tensor imaging (DTI) and volumetry. *Cerebral Cortex*, 20(9), 2055–2068. <https://doi.org/10.1093/cercor/bhp280>
- Yeatman, J. D., Wandell, B. A., & Mezer, A. A. (2014). Lifespan maturation and degeneration of human brain white matter. *Nature Communications*, 5, 4932–4932. <https://doi.org/10.1038/ncomms5932>
- Yu, F., Fan, Q., Tian, Q., Ngamsombat, C., Machado, N., Bireley, J. D., ... Huang, S. Y. (2019). Imaging G-ratio in multiple sclerosis using high-gradient diffusion MRI and macromolecular tissue volume. *American Journal of Neuroradiology*, 40(11), 1871–1877. <https://doi.org/10.3174/ajnr.A6283>
- Zhang, H., Schneider, T., Wheeler-Kingshott, C. A., & Alexander, D. C. (2012). NODDI: Practical in vivo neurite orientation dispersion and density imaging of the human brain. *NeuroImage*, 61(4), 1000–1016. <https://doi.org/10.1016/j.neuroimage.2012.03.072>
- Zhang, J., Kolind, S. H., Laule, C., & MacKay, A. L. (2015a). Comparison of myelin water fraction from multiecho T2 decay curve and steady-state methods. *Magnetic Resonance in Medicine*, 73(1), 223–232. <https://doi.org/10.1002/mrm.25125>
- Zhang, J., Kolind, S. H., Laule, C., & MacKay, A. L. (2015b). How does magnetization transfer influence mcDESPT results? *Magnetic Resonance in Medicine*, 74(5), 1327–1335. <https://doi.org/10.1002/mrm.25520>

How to cite this article: Bouhrara M, Kim RW, Khattar N, et al. Age-related estimates of aggregate g-ratio of white matter structures assessed using quantitative magnetic resonance neuroimaging. *Hum Brain Mapp*. 2021;42: 2362–2373. <https://doi.org/10.1002/hbm.25372>